

# Early Triassic super-greenhouse climate driven by vegetation collapse

Zhen Xu (✉ [janexu@cug.edu.cn](mailto:janexu@cug.edu.cn))

China University of Geosciences (Wuhan); University of Leeds

Jianxin Yu

China University of Geosciences (Wuhan)

Hongfu Yin

China University of Geosciences

Andrew Merdith

University of Leeds <https://orcid.org/0000-0002-7564-8149>

Jason Hilton

University of Birmingham <https://orcid.org/0000-0003-0286-8236>

Bethany Allen

ETH Zürich; Swiss Institute of Bioinformatics

Paul Wignall

University of Leeds

Alexander Dunhill

University of Leeds

Khushboo Gurung

University of Leeds

Jun Shen

China University of Geosciences <https://orcid.org/0000-0003-3759-6533>

David Schwartzman

Howard University

Yves Godderis

Geoscience Environnement Toulouse <https://orcid.org/0000-0002-6054-614X>

Yannick Donnadieu

CEREGE <https://orcid.org/0000-0002-7315-2684>

Yuxuan Wang

University of Leeds

Yinggang Zhang

School of Earth Sciences and Engineering, Nanjing University

Simon Poulton

University of Leeds <https://orcid.org/0000-0001-7621-189X>

Benjamin Mills

## Physical Sciences - Article

### Keywords:

**Posted Date:** September 23rd, 2022

**DOI:** <https://doi.org/10.21203/rs.3.rs-2084887/v1>

**License:**   This work is licensed under a Creative Commons Attribution 4.0 International License.

[Read Full License](#)

---

# Abstract

The Permian–Triassic Mass Extinction (PTME), life’s most severe crisis<sup>1</sup>, has been attributed to intense global warming triggered by CO<sub>2</sub> emissions from Large Igneous Province volcanism<sup>2–8</sup>. It remains unclear, however, why super-greenhouse conditions persisted for around five million years after the volcanic episode, when Earth system feedbacks should have returned temperatures to pre-extinction levels within a few hundred thousand years<sup>8</sup>. Here we use fossil occurrences and lithological indicators of climate to reconstruct spatio-temporal maps of plant productivity and biomass changes through the Permian–Triassic and undertake climate-biogeochemical modelling to investigate the unusual longevity and intensity of warming. Our reconstructions show that terrestrial vegetation collapse during the PTME, especially in tropical regions, resulted in an Earth system with low levels of organic carbon sequestration and chemical weathering, leading to limited drawdown of greenhouse gases. This led to a protracted period of extremely high surface temperatures, during which biotic recovery was delayed for millions of years. Our results support the idea that thresholds exist in the climate-carbon system beyond which warming may be amplified substantially.

## Full Text

The latest Permian to Early Triassic (~252–247 million years ago; Ma) was a period of intense environmental and biotic stress<sup>1</sup>. During the Permian–Triassic Mass Extinction (PTME) at ~252 Ma, around 90% of species in terrestrial and marine settings became extinct<sup>1</sup>, with substantial recovery only starting around five million years later in the Middle Triassic<sup>8,10,11</sup>. It is generally agreed that the PTME was driven by volcanogenic carbon emissions from Siberian Traps volcanism, potentially coupled with additional thermogenic releases, resulting in intense greenhouse warming<sup>2–8,12</sup>. A major negative excursion in carbonate  $\delta^{13}\text{C}$  ratios, over a time interval of about 50–500 thousand years (kyrs), supports the notion of a major carbon cycle perturbation<sup>8,13</sup>. However, it is much less well understood why the extreme hothouse climate persisted throughout the 5 million years (Myrs) of the Early Triassic.

The precise time interval of Siberian Traps degassing is uncertain, although the main phase of volcanism occurred around the Permian-Triassic Boundary (PTB), possibly with a further pulse about two million years later, during the Smithian Substage<sup>10</sup>. Nevertheless, it is expected that atmospheric CO<sub>2</sub> and global surface temperature would have declined to pre-extinction levels within ~100 kyr of volcanic pulses, due to amplified global silicate weathering and increased burial of organic carbon<sup>8</sup>. Thus, some critical factor (or combination of factors) is missing from our current conceptual understanding of the Permo–Triassic hothouse, which facilitated the persistence of extreme temperatures for ~5 Myrs following the PTME.

One proposed solution for this “missing factor” is the inability of the silicate weathering thermostat to remove sufficient CO<sub>2</sub> due to a limited availability of fresh, weatherable material<sup>14</sup>. This is based on existence of a theoretical maximum weathering rate set by the supply of cations from denudation<sup>15,16</sup>,

but if weathering rates were limited in this way following the PTB, CO<sub>2</sub> levels would have been expected to either increase out of control, or decrease monotonically<sup>16</sup>. However, the protracted and relatively stable high temperatures of the Early Triassic<sup>12</sup> imply that climate was indeed being regulated by silicate weathering, and linked climate-weathering models that estimate the global supply of cations do not support a ‘maxing out’ of the silicate weathering feedback, even if Early Triassic CO<sub>2</sub> levels exceeded 10,000 ppm<sup>17,18</sup>.

An alternative solution for elevated Early Triassic temperatures is an ‘upper temperature steady state’, in which some change in the Earth system caused the climate-carbon cycle to stabilize at a much higher global temperature for millions of years<sup>19</sup>. In this regard, a potential driver is the dramatic and prolonged reduction of terrestrial biomass caused by the PTME<sup>1</sup>. Peat-forming ecosystems are responsible for substantial drawdown of CO<sub>2</sub>, but these extensive biomes were lost at the end of the Permian<sup>12,20–22</sup>. Plant species richness and abundance dropped significantly during the Permo–Triassic transition, leaving a ~7 million year “coal gap” in the Early to Middle Triassic<sup>20,21</sup>

Here, we quantitatively estimate the distribution of terrestrial plant biomass across the PTME and Early-to-Mid Triassic from the plant fossil record, and use this information to guide a linked climate-biogeochemical model of the Early Triassic hothouse, in order to test whether these biotic changes may have resulted in a higher temperature steady state. Our plant fossil database, including macrofossil and palynology data from the end Permian to the Middle Triassic, is detailed in the Supplementary Information Table S4 and S5. As fossil plants are typically fragmented prior to fossilization, all plant fossil records have been normalized<sup>23</sup> to reduce artefacts of palaeobotanical nomenclature (see Methods for details). Normalization compensates for the palaeobotanical practice of assigning different plant organs (e.g., roots, stems, leaves, cones and seeds) of the same plant to separate fossil genera and species<sup>21</sup>. For each plant group, we selected the most representative plant organ to analyze and omitted other organs that belong to the same plant group, to avoid duplication<sup>23</sup>. For example, for tree lycopods we used species of the stem genus *Lepidodendron*, which are the most common fossils and are readily distinguished from one another, and we excluded other organs from tree lycopods, including their cones, sporophylls (fertile leaves) and leafy branches and leaves that carry different genus and species names<sup>21</sup>.

Diversity estimates and inferences from plant morphology were used to construct climate-linked plant biomes. Floral character and function analysis of different palaeogeographic regions were partly based on macrofossil family level clustering, and partly on the species richness in each morphological category<sup>24</sup>. Floras were matched using the Köppen-Geiger climate classification system, which is based on the proportion of taxa within each habitat. For example, gigantopterids lived in rainforests<sup>25</sup>, so flora with a high fraction of gigantopterid species were deemed more likely to represent rainforest climate zones (see Supplementary Information). Our results, shown in Figure 1, highlight the more substantial extinction of low–middle latitude (–45°–45°) tropical–subtropical vegetation during the PTME, with 86% species extinction in low–middle latitudes, as opposed to 66% in high latitudes (see Table S1). Before the

PTME, plant species richness was greatest in low–mid latitude areas, while after the crisis, species richness in high latitude areas was much higher (Fig. 1-B). This reversal of the modern latitudinal diversity gradient is also seen in terrestrial tetrapods after the PTME<sup>26</sup>.

The key terrestrial palaeophytogeographical features of the Permian–Triassic interval are the replacement of the low-latitude tropical Cathaysian flora, low–middle latitude temperate–subtropical Euramerica flora, high-latitude boreal Angara flora, and meridional Gondwana flora, by a uniform herbaceous lycopod-dominated flora in the Early Triassic<sup>8,21,27</sup> (Fig. 1-A). High latitude areas, such as Siberia, provided a refuge, while the expansion of high temperature and seasonal aridity saw the loss of most plants in lower latitudes during the Early Triassic<sup>21,28–30</sup>. After the inhospitable Induan stage (251.9–249.9 Ma), plants gradually migrated from high to middle-low latitude areas during the Olenekian stage (249.9–246.7 Ma). Further recovery in the Middle Triassic Anisian stage (246.7~241.5 Ma), saw tropical biomes reappear at low palaeolatitudes<sup>21</sup> (Fig. 2).

The plant fossil occurrences were combined with fossil tetrapod occurrences and lithological indicators of local climate (e.g. coals, evaporites, tillites), and transferred onto a palaeogeographic grid map<sup>31</sup>. These data were then used to extrapolate across corresponding climate zones. To produce a map of palaeo-biomass from our distribution of biomes, we rely on evidence from the present<sup>32</sup>. The latest Permian Changhsingian stage (254.2–251.9 Ma) had a similar atmospheric CO<sub>2</sub> concentration to the present day<sup>4</sup>. Thus, it has been assumed that the net primary productivity on land (NPPL) would not have been higher than the modern world, at about 60 Pt C/yr<sup>33</sup>. The NPPL of each grid cell in our palaeogeographic reconstructions (Fig. 2) was determined using the nearest living flora that shares a similar basic physiology, geographic location and climate zone, assuming that the growth and transpiration rate of the dominant Palaeozoic taxa are comparable to extant gymnosperms and angiosperms<sup>32,34</sup> (see Supplementary Information). Our reconstruction suggests that global terrestrial primary productivity fluctuated from ~54.8–58.9 Pt C/yr in the latest Permian Changhsingian, to a low of ~16.9–20.5 Pt C/yr in the Early Triassic Induan (a loss of ~65%), followed by Olenekian values of ~40.0–45.6 Pt C/yr, with ~69.1–74.2 Pt C/yr in the Middle Triassic Anisian. Before the PTME, the global terrestrial productivity gradient correlated with latitude, with the highest values in the tropics, similar to the modern world<sup>33</sup>. However, this trend dramatically reverses following the PTME as regions of high productivity migrated from low-to-high latitudes, before gradually re-establishing the previous gradient during the Olenekian and Anisian stages.

To test the biogeochemical and climatic effects of these shifts in plant productivity, we use our palaeobiogeographic reconstructions as inputs to the *SCION* Earth Evolution Model<sup>18,35</sup>. *SCION* is a global climate-biogeochemical model that links steady-state 3D climate<sup>17</sup> and surface processes to a biogeochemical box model<sup>36</sup>. It calculates continental weathering rates at each grid point on the land surface based on local temperature, runoff and erosion rates, as well as an assumed biotic enhancement factor. We modified the biotic enhancement factor based on the NPPL in each grid cell, allowing for a 4-fold enhancement between the most and least productive grid cells as a conservative estimate (see refs.

37–39 for a range of estimates of this factor and the SI for model runs with different factors). In addition to modifying the continental weathering routine, we summed the total NPPL for each time period and used this to replace the model calculation of global terrestrial NPPL and to scale the flux of terrestrially-derived organic carbon burial (see Supplementary Information for details and [github.com/bjwmills/SCION](https://github.com/bjwmills/SCION) for the SCION code and documentation).

Palaeozoic forests were dominated by spore-producing plants like *Lepidodendron* with the potential for rapid growth and short lifespans, thriving in peat-forming environments with low pH substrates that facilitated preservation of vegetation litter<sup>40,41</sup>. By contrast, Mesozoic forests were dominated by long-lived gymnosperms, which grew slowly once mature, typically in upland settings with less litter preservation. These Mesozoic forests represent a saturated carbon sink, and so may have been less efficient in transferring atmosphere CO<sub>2</sub> into stable bio-carbon<sup>40,42</sup>. To represent this potential difference between Palaeozoic and Mesozoic plant groups, as well as enhanced aridity after the PTME, we defined a new parameter, “Preservation efficiency”, when applying the global NPPL data to organic carbon burial in *SCION*. Here we assume that the preservation of Palaeozoic vegetation was twice as efficient as for Mesozoic vegetation<sup>42</sup>. Functionally, this alteration does not affect model results for our period of interest (see SI for comparisons), but it allows the model to more accurately reconstruct the Permian high-carbon-burial environment and to capture the high carbonate  $\delta^{13}\text{C}$  values observed before the extinction event.

Aside from these changes, the model retains the Phanerozoic-scale forcing information from previous standard runs<sup>18</sup>, including background tectonic CO<sub>2</sub> degassing. The only abiotic alteration to the model was to include additional CO<sub>2</sub> degassing from the Siberian Traps<sup>8</sup>, which accurately reproduces the shorter term (~500 kyr) carbon isotope perturbations across the PTME. As with previous *SCION* runs, we performed a standard sensitivity ensemble, varying the degassing rate and isotopic fractionation effects through their uncertainty ranges<sup>18</sup>.

Figure 3 shows the *SCION* model results through the latest Permian, and the Early and Middle Triassic, both with and without the inclusion of our palaeo-vegetation constraints. In the default run (dashed line), the NPP of each continental grid cell is kept constant at 420 g C/m<sup>2</sup>/yr to produce an overall productivity similar to our late Permian fossil-constrained vegetation map, and all changes in the model environment are driven by abiotic forcings, such as background tectonic degassing rates and the Siberian Traps degassing. The major features of this default run are the spikes in CO<sub>2</sub> concentration and temperature (Fig. 3-D, F), and the accompanying  $\delta^{13}\text{C}$  excursion (Fig. 3-C), driven by the Siberian Traps degassing. The magnitude of the isotope excursion is consistent with data from geochemical proxies and previous modelling<sup>43</sup>, and CO<sub>2</sub> concentration rises from about 2,000 to 4,000 ppm, with a corresponding increase in equatorial surface temperature of about 3°C. The high background CO<sub>2</sub> level and relatively small temperature increase are both features of the low climate sensitivity in the *FOAM* climate model<sup>44</sup>, which provides the steady state 3D climate for *SCION*. Thus, we expect that a more complex model might allow for a more dramatic temperature increase and lower overall CO<sub>2</sub> levels, as suggested by proxy data<sup>4,7,12</sup>.

However, no amount of climate model complexity can account for the data-model mismatch during the Early Triassic, where model temperatures decline immediately after the cessation of Siberian Traps emissions. Because *SCION* has a single-box ocean, it does not balance sub-million-year alkalinity and shallow sea carbonate deposition as accurately as multi-box models, in which CO<sub>2</sub> levels decline even more rapidly<sup>43</sup>.

When included in the model, the ~65% loss in vegetation productivity from the End Permian to Early Triassic, and the related effects on continental weathering, result in a sustained high atmospheric CO<sub>2</sub> content<sup>4</sup> and high Early Triassic temperatures (green areas in Figure 3). In these model runs, the reduction in terrestrial organic carbon burial and nullification of silicate weathering result in CO<sub>2</sub> levels stabilizing at up to 10,000 ppm, with mean equatorial surface temperatures of around 33–34°C over a 5 Myr period, which is consistent with proxy inferences<sup>4,7,12</sup> (Fig. 3). The Early Triassic δ<sup>13</sup>C level is also reduced by around 2‰ compared to the default run, generally improving the fit to the geologic record. Two exceptions to this are the Induan-Olenekian (Dienerian-Smithian) boundary and the late Olenekian (early Spathian), which are marked by transient positive carbon isotope excursions that may have been driven by increasing marine productivity, transgression, or marine anoxia<sup>10,45–47</sup> which are not considered in our model. The prolonged hothouse environment is terminated by the progressive terrestrial ecosystem recovery, starting in the Olenekian but accelerating in the Anisian, which is also consistent with the observed uptick in δ<sup>13</sup>C values across the Olenekian – Anisian boundary and the cooling which occurred during this time<sup>12</sup>. This dynamic fits with broader evidence for a more benign environment for the re-establishment of land and marine ecosystems in the Middle Triassic<sup>11,46</sup>.

In our model scenario, the effect of plants on continental silicate weathering is more capable of driving an increase in atmospheric CO<sub>2</sub> than the direct limitation of organic carbon burial (see Figs. S1 and S2). This is because while the large reduction in terrestrially-derived organic carbon burial acts to increase CO<sub>2</sub> levels, it also decreases atmospheric oxygen levels and redistributes nutrients to the ocean, meaning that more marine organic carbon is produced and preserved, and less fossil organic carbon is weathered. It is possible that these negative feedbacks on the organic carbon cycle are overly-strong in the *SCION* model, which may be why it fails to replicate the degree of variation in Phanerozoic atmospheric O<sub>2</sub> (ref. 18). Additionally, the weathering of sedimentary organic carbon likely increases with temperature<sup>48</sup>, which is not accounted for in the model, and may nullify these negative feedbacks further. Thus, a more complete model may well predict even higher surface temperatures, consistent with the proxy data. A further uncertainty in our modelling is the degree to which plants amplify continental weathering, but as shown in figure S3, the 'best guess' values from Phanerozoic scale models of a 4-7 fold enhancement<sup>18,39</sup> all produce outcomes consistent with the geological record.

Our study provides a novel quantitative estimation of changes to global palaeo-plant biomass and the corresponding long-term environmental impact. Through our modelling, we show that the large decrease in plant productivity in the terrestrial biosphere, especially in the tropics, resulted in a world that was extremely hot by the standards of the Phanerozoic, a consequence of substantially weakened carbon

sequestration rates. These conditions persisted for millions of years and cooling was only achieved as plant productivity began to increase at all latitudes. This demonstrates that thresholds exist in the Earth system that can accelerate climate change and have the potential to maintain adverse climate states for millions of years, with dramatic implications for global ecosystem behavior. The potential impacts of these climate thresholds for human civilization are also stark: it is well-understood that without future techniques to remove of CO<sub>2</sub>, humans will be living with elevated surface temperatures for up to 100 thousand years<sup>49,50</sup>. If current warming leads to the destruction of the tropical rainforests, then it is entirely plausible that this long-term trend may be towards higher, rather than cooler surface temperatures.

## References

1. Wignall, P.B. *The Worst of Times: How Life on Earth Survived 80 Million Years of Extinction* (Princeton Univ. Press, Princeton, 2015).
2. Svensen, H. et al. Siberian gas venting and the end-Permian environmental crisis. *Earth Planet. Sci. Lett.* **277**, 490–500 (2009).
3. Joachimski, M.M. et al. Climate warming in the latest Permian and the Permian-Triassic mass extinction. *Geology* **40**, 195–198 (2012).
4. Joachimski, M.M. et al. Five million years of high atmospheric CO<sub>2</sub> in the aftermath of the Permian–Triassic mass extinction. *Geology* **50**, 650–654 (2022).
5. Burgess, S.D., Muirhead, J.D., & Bowring, S.A. Initial pulse of Siberian Traps sills as the trigger of the end-Permian mass extinction. *Nat. Commun.* **8**, 164 (2017).
6. Shen, J. et al. Evidence for a prolonged Permian–Triassic Extinction interval from global marine mercury records. *Nat. Commun.* **10**, 1563 (2019).
7. Wu, Y.Y. et al. Six-fold increase of atmospheric pCO<sub>2</sub> during the Permian-Triassic mass extinction. *Nat. Commun.* **12**, 2137 (2021).
8. Dal Corso, J. et al. Environmental crises at the Permian–Triassic mass extinction. *Nat. Rev. Earth Environ.* **3**, 197–214 (2022).
9. Kemp, L. et al. Climate Endgame: Exploring catastrophic climate change scenarios. *Proc. Natl. Acad. Sci. U. S. A.* **119**(34), e2108146119 (2022).
10. Payne, J.L. et al. Large perturbations of the carbon cycle during recovery from the end-Permian extinction. *Science* **305**, 506–509 (2004).
11. Song, H., Wignall, P.B., & Dunhill, A.M. Decoupled taxonomic and ecological recoveries from the Permo-Triassic extinction. *Sci. adv.* **4**(10), eaat5091 (2018).
12. Sun, Y.D. et al. Lethally hot temperatures during the Early Triassic greenhouse. *Science* **338**, 366–370 (2012).
13. Jurikova, H. et al. Permian–Triassic mass extinction pulses driven by major marine carbon cycle perturbations. *Nat. Geosci.* **13**, 745–750 (2020).

14. Kump, L.R. Prolonged Late Permian–Early Triassic hyperthermal: failure of climate regulation? *Phil. Trans. R. Soc. A.* **376**, 20170078 (2018).
15. West, A.J., Galy, A., & Bickle, M. Tectonic and climatic controls on silicate weathering. *Earth Planet. Sci. Lett.* **235**, 211–228 (2005).
16. Mills, B.J.W. et al. Timing of Neoproterozoic glaciations linked to transport-limited global weathering. *Nat. Geosci.* **4**, 861–864 (2011).
17. Godd ris, Y. et al. The role of paleogeography in the Phanerozoic history of atmospheric CO<sub>2</sub> and climate. *Earth-Sci. Rev.* **128**, 122–138 (2014).
18. Mills, B.J.W., Donnadieu, Y., & Godd ris, Y. Spatial continuous integration of Phanerozoic global biogeochemistry and climate. *Gondwana Res.* **100**, 73–86 (2021b).
19. Mills, B.J.W., Tennenbaum, S., & Schwartzman, D. Exploring multiple steady states in Earth's long-term carbon cycle. *Am. J. Sci.* **321**, 1033–1044 (2021a).
20. Retallack, G.J., Veevers, J.J., & Morante, R. Global coal gap between Permian–Triassic extinction and Middle Triassic recovery of peat-forming plants. *Geol. Soc. Amer. Bull.* **108**, 195–207 (1996).
21. Xu, Z. et al. End Permian to Middle Triassic plant species richness and abundance patterns in South China: Coevolution of plants and the environment through the Permian–Triassic transition. *Earth-Sci. Rev.* **232**, 104136 (2022).
22. Benton, M.J., & Newell, A.J. Impacts of global warming on Permo-Triassic terrestrial ecosystems. *Gond. Res.* **25**, 1308–1337 (2014).
23. Cleal, C.J. et al. Paleobotanical experiences of plant diversity in deep time. 1: How well can we identify past plant diversity in the fossil record? *Palaeogeogr. Palaeoclimatol. Palaeoecol.* **576**, 110481 (2021).
24. Rees, P. M. et al. Permian phytogeographic patterns and climate data/model comparisons. *J. Geology* **110**, 1–31 (2014).
25. Yu, J.X. et al. Vegetation changeover across the Permian-Triassic boundary in Southwest China extinction, survival, recovery and paleoclimate: a critical review. *Earth-Sci. Rev.* **149**, 203–224 (2015).
26. Allen, B.J., Wignall, P.B., Hill, D.J., Saupe, E.E., & Dunhill, A.M. The latitudinal diversity gradient of tetrapods across the Permo-Triassic mass extinction and recovery interval. *Proc. R. Soc. B: Biol. Sci.* **287**, 20201125 (2020).
27. Grauvogel-Stamm, L., & Ash, S.R. Recovery of the Triassic land flora from the End-Permian life crisis. *Comptes. Rendus. Palevol.* **4**, 593–608 (2005).
28. MacLeod, K.G., Quinton, P.C., & Bassett, D.J. Warming and increased aridity during the earliest Triassic in the Karoo Basin, South Africa. *Geology* **45**, 483–486 (2017).
29. Cui, C.Q., & Cao, C. Increased aridity across the Permian–Triassic transition in the mid-latitude NE Pangea. *Geol. J.* **56**, 6162–6175 (2021).
30. Davydov, V.I. et al. Climate and biotic evolution during the Permian–Triassic transition in the temperate Northern Hemisphere, Kuznetsk Basin, Siberia, Russia. *Palaeogeogr. Palaeoclimatol.*

- Palaeoecol.* **573**, 110432 (2021).
31. Boucot, A.J., Chen, X., Scotese, C.R., & Morley, R.J. Phanerozoic paleoclimate: an atlas of lithologic indicators of climate. *SEPM (Society for Sedimentary Geology)* **11**, (2013).
  32. Wilson, J.P. et al. Dynamic Carboniferous tropical forests: new views of plant function and potential for physiological forcing of climate. *New Phytologist* **251**, 1333–1353 (2017).
  33. Beerling, D., & Woodward, F.I. Vegetation and the terrestrial carbon cycle: modelling the first 400 million years (Cambridge Univ. Press, Cambridge, 2001).
  34. Sitch, S. et al. Evaluation of ecosystem dynamics, plant geography and terrestrial carbon cycling in the LPJ dynamic global vegetation model. *Glob. Change Bio.* **9**, 161–185 (2003).
  35. Longman, J. et al. Assessing volcanic controls on Miocene climate change. *Geophys. Res. Lett.* **49**(2), e2021GL096519 (2022).
  36. Tostevin, R., & Mills, B.J. Reconciling proxy records and models of Earth's oxygenation during the Neoproterozoic and Palaeozoic. *Interface Focus* **10**, 20190137 (2020).
  37. Lenton, T.M., & von Bloh, W. Biotic feedback extends the life span of the biosphere. *Geophysical Res. Lett.* **28**, 1715–1718 (2001).
  38. Berner, R.A., VandenBrooks, J.M., & Ward, P.D. Oxygen and evolution. *Science* **316**, 557–558 (2007).
  39. Lenton, T.M. Daines, S.J., & Mills, B.J.W. COPSE reloaded: an improved model of biogeochemical cycling over Phanerozoic time. *Earth-Sci. Rev.* **178**, 1–28 (2018).
  40. Cleal, C.J., & Thomas, B.A. Paleozoic tropical rainforests and their effect on global climates: is the past the key to the present? *Geobio.* **3**, 13–31 (2005).
  41. Beaulne, J., Garneau, M., Magnan, G., & Boucher, É. Peat deposits store more carbon than trees in forested peatlands of the boreal biome. *Sci. Rep.* **11**, 2657 (2021).
  42. Boyce, C.K., & DiMichele, W.A. Arborescent lycopsid productivity and lifespan: Constraining the possibilities. *Rev. Palaeobot. Palynol.* **227**, 97–110 (2016).
  43. Dal Corso, J. et al. Permo-Triassic boundary carbon and mercury cycling linked to terrestrial ecosystem collapse. *Nat. Commun.* **11**, 2962 (2020).
  44. Jacob, R. et al. Computational design and performance of the Fast Ocean Atmosphere Model, version one. In International Conference on Computational Science (pp. 175–184). Springer, Berlin, Heidelberg (2001).
  45. Song, H. et al. Anoxia/high temperature double whammy during the Permian-Triassic marine crisis and its aftermath. *Sci. Rep.* **4**, 1–7 (2014).
  46. Shen, J., Schoepfer, S.D., Feng, Q., & Song, H.Y. Marine productivity changes during the End-Permian crisis and Early Triassic recovery. *Earth-Sci. Rev.* **149**, 136–162 (2015).
  47. Sun, Y.D. et al. Integrated bio-chemostratigraphy of Lower and Middle Triassic marine successions at Spiti in the Indian Himalaya: Implications for the Early Triassic nutrient crisis. *Glob. Planet. Chang.* **196**, 103363 (2021).

48. Soulet, G. et al. Temperature control on CO<sub>2</sub> emissions from the weathering of sedimentary rocks. *Nature Geosci.* **14**, 665-671 (2021).
49. Archer, D. et al. Atmospheric lifetime of fossil fuel carbon dioxide. *Annu. Rev. Earth Planet. Sci.* **37**, 117–134, (2009).
50. Lord, N.S., Ridgwell, A., Thorne, M.C., & Lunt, D.J. An impulse response function for the “long tail” of excess atmospheric CO<sub>2</sub> in an Earth system model. *Glob. Biogeochem. Cycles* **30**(1), 2–17, (2016).

## Methods

The geological timings used in this paper are from Geological Time Scale (GTS) 2020<sup>51</sup>.

### Plant macrofossil and palynology data normalization steps

Plant macrofossils are typically fragmented into different parts (organs) prior to fossilization, with each part typically named separately using Linnean binomials<sup>23</sup>. We normalized the dataset to correct for potential duplications in which different parts of the same plant may be included under different species or genus names. In normalization, organs such as species or genera of seeds, trunks, roots and leaves are removed from the dataset if another, more identifiable or morphological diverse organ produced by the same plant is present, so that each whole plant is counted only once. For diverse leaf groups, for example ferns and sphenophytes, leaf species or genera are used, as these fossils typically lack more distinctive organs with suitable preservation. An example is the diverse trunk group of tree lycopods, where species of *Lepidodendron* are used as they are abundant and systematically informative<sup>23,52</sup>, rather than other organs produced by the same plant, including cones, sporophylls (fertile leaves) or roots (see ref. 21 for detail). Indeterminate species denoted as “sp.” of an existing genus are regarded as poorly preserved examples of the existing species of that genus, and are deleted. If the indeterminate species is the only species in that genus, they are counted as a single, unnamed species of that genus. Normalized macro plant fossil species data is listed in Table S4. In strata lacking plant macrofossils, palynological occurrences are taken into account.

### Macro fossil plant species extinction magnitude

All the species occurrences presented are based on the normalized data (Table S4). Longitude and latitude for each fossil location are listed in Table S5. The high latitude area is defined to be >45 degrees north and south of the equator, while low-middle latitude area is <45 degrees north or south. The range of plant fossils in each stage was checked and extended for calculating the extinction magnitude over a global high-latitude and low–middle latitude area. The extinction magnitude for each stage is the extinct

species number compared to a later stage, minus the total normalized species number of this stage. See the extinction rate results in Supplementary Information Table S1.

### **Flora characterization by clustering and morphological group**

To analyze the character of floras from the end Permian (Changhsingian) to Middle Triassic (Anisian), family level clustering was used with the normalized plant fossil data. The clustering result is based on the Euclidean method. The plant systematic information comes from the Global Biodiversity Information Facility (GBIF) <https://www.gbif.org/> database, with additions from the literature listed in the Supplementary Information. The taxonomic affinity of most spores and pollens are unknown, and so only plant macrofossil data was used in clustering, and the palynology data was only used in the morphological group diversity analysis. To show the uncertainty of the clustering results, we list the plant species number after each flora in Figure 1-A. Unsurprisingly, the clustering results for flora with fewer taxa were less reliable and more crowded together. As an auxiliary method to clustering, we counted the plant species number in each morphological group (see the fourteen morphological group classifications below), then calculated the proportion of the species number in each morphological group within floras to directly show the character and to construct a representative pie chart for each flora. For flora with fewer taxa, we adjusted the location of each flora in the clustering tree manually, according to the character shown by the morphological group diversity.

Plants were divided into six habitats and fourteen groups, including four arid types: conifer, gymnosperm (for seed plants where systematic class/group is uncertain), peltasperm and seed fern; three humid highland types: cordaites, ginkgophyte, cycadophyte; one rainforest type: gigantopterid; two humid types: fern and 'fern2' (for taxa that could be either ferns or seed fern); two marsh types: sphenophyte and lycopod; one cold type: glossopterid – normally reported in boreal Gondwana; and one coastal type: herbaceous lycopod. Flora dominated by one habitat group was classified into the corresponding climate zone, and flora with more than one habitat group was defined as a mixture. In this step, we also took flora without a macrofossil record but with palynology data into account. The group information of the in-situ spore and pollen producing plant were counted<sup>53</sup>. For flora with both plant macrofossil and palynology data, we chose the dataset which contains more information. In Figure 1-A, flora with more than 150 taxa, such as the Changhsingian South China flora, have the biggest pie chart area, while flora with less than 10 taxa, like the German flora, have the smallest pie chart. After the clustering and morphological group counting analysis, the character of the flora from the End Permian to the Middle Triassic was systematically studied and classified into climate zones as shown in Table S2.

### **Vegetation biomass reconstruction**

Terrestrial tetrapod data was used to infer the occurrence of plants on regions without a plant fossil record. Generally terrestrial tetrapod occurrences in our study coincided with the occurrences in the plant fossils, except for the Olenekian record in America and Canada. Therefore, vegetation type in those areas at this time was inferred from the tetrapod information alone (Supplementary Information Table S6).

Global vegetation was reconstructed by extension of fossil flora data across appropriate climate zones indicated by a sedimentary climate map<sup>31</sup>. In arid and polar areas, plant fossil extrapolation is restricted<sup>12,54</sup>. Extrapolation was not carried out at the boundaries of humid and arid environments in places that lacked supporting mineralogical data. For example, the Early and Middle Triassic low-latitude inner Pangean continent is inferred to have been arid savanna or steppe, based on the available fossil record and lithological climatic indicators. Fossils from more productive biomes which are found nearer the coast are therefore not extrapolated far into the continental interior where climate is arid, but are restricted to the coastline (Fig. 2).

Three principles are used for functional comparison between ancient and recent floras to estimate palaeo-biomass: firstly, recent floras must have a similar physiology or function to the ancient flora we wish to imitate, so we prefer C3 plants and not angiosperms. Secondly, the recent and ancient floras should be in the same climate zone and similar geographic location, for example, the latest Permian South China tropical forest was a low-latitude island, and so present-day, large tropical islands like Indonesia and Thailand were chosen over (for example) continental Brazil. Thirdly, the chosen flora should fit in the global diversity and NPP gradient at a similar place to the ancient flora. For instance, the end Permian (Changhsingian) tropical South China flora has the highest diversity, and is matched with a present day high-diversity, high-productivity biome, that of present day Thailand. The NPP of each ancient flora is listed in Table S2 and details of corresponding recent flora are in Table S3.

## Palaeogeographic reconstruction

To reconstruct the spatial vegetation map, we assembled a database of fossil locations, plant macrofossil, palynology and terrestrial tetrapod data for our time periods (Table S5). The fossil locations were then reconstructed to their time of deposition using *GPlates*<sup>55</sup>. Because the palaeogeographic reconstruction used in *SCION*<sup>56</sup> has no available set of reconstruction files, we used the reconstruction files of Macdonald<sup>57</sup>, whose reconstruction at ~250 Ma is similar to that of ref. 56. This allowed us to place fossil locations in an internally correct position at 250 Ma. However, minor manual manipulation was needed to then map some of these locations to their correct corresponding positions in the *SCION* land-sea maps.

## Plant latitudinal diversity calculation

To investigate the influence of plant fossil sampling completeness on our estimates of diversity, squares and interpolation methods were applied to our normalized plant macrofossil occurrence data. As for the raw data, squares and interpolation were applied to 15° latitude bins for the Late Permian (Changhsingian) to Middle Triassic (Anisian). Coverage-based interpolation uses the abundance structure present within samples, to either subsample or extrapolate diversity estimates to particular levels of sampling completeness, known as quorum levels<sup>26,58,59</sup>. This was applied using the R package iNEXT<sup>58</sup>. Squares is an extrapolator based on the proportion of singletons in a sample, and is thought to be more robust to biases associated with small sample sizes and uneven abundance distributions<sup>60,61</sup>.

Throughout the interval, the raw, squares and interpolated diversity estimates generally show similar latitudinal patterns, suggesting that sampling is not particularly uneven across space in our dataset (Figure 1-B). However, many of the points in the interpolated curves were removed due to over-extrapolation, which indicates that many of the spatio-temporal bins may be under-sampled. Our results indicate that during the Induan, the highest plant diversity was found in the high latitudes, particularly in the northern hemisphere. However, during the Changhsingian, Olenekian and Anisian, we see higher diversity levels at tropical latitudes, suggesting that the latitudinal diversity gradient had reverted to a situation similar to that of the present day.

## Climate-biogeochemical modelling

To investigate the effects of vegetation change on Early Triassic climate, we ran the SCION Earth Evolution Model<sup>18</sup>. We removed the equation which calculates terrestrial vegetation biomass (as a single global number) and replaced this with our reconstruction, mapped onto the model continental surface. We altered the model parameter  $f_{biota}$  which represents the biotic enhancement of continental weathering (again a single number in SCION), to make this dependent on the local vegetation biomass in the following way:

$$f_{biota} = 0.002 \cdot NPP + 0.25$$

Functionally, this returns tending towards 0.25 when biomass is very low, and a linear scaling with NPP when biomass rises. The choice of 0.25 relates to the four-fold enhancement between simple ground covers and higher plants used in first-generation long-term carbon cycle models such as GEOCARB<sup>62,63</sup>, and based on field and laboratory studies<sup>37</sup>. We vary this 'preplant' factor between 0.15 – 1 in the SI and modify the linear scaling to account for this. In all formulations, the scaling factor for NPP is chosen to return present day global weathering rates.

We defined land-derived organic carbon burial as:

$$k_{locb} \cdot \frac{P_{land}}{P_{land0}} \cdot k_{preservation}$$

where  $k_{locb}$  is the present-day rate of land-derived organic carbon burial,  $P_{land}$  is the phosphorus delivery to land,  $P_{land0}$  is the present-day phosphorus delivery, and  $k_{preservation}$  is an arbitrary multiplier set to 2 in the Palaeozoic and 1 in the Mesozoic, to represent better preservation of Palaeozoic organic matter (see text), and allowing the model to replicate high Permian carbonate  $\delta^{13}\text{C}$ .

### Data availability

The normalized plant and land tetrapod data taxa list and occurrence are provided in Supplementary Information Tables S4–S6. The normalization details are available from Zhen Xu on request.

### Code availability

Full SCION model code and documentation is available at <https://github.com/bjwmills/SCION>. Open access preprints for papers describing all model versions and derivations are available at [bjwmills.com](http://bjwmills.com).

[the model code version used for this work is attached to this paper submission and will be available online if the paper is published]

### Further References

51. Gradstein, F.M., Ogg, J.G., Schmitz, M.D., & Ogg, G.M. (Eds.) Geological time scale 2020 (Elsevier, Netherlands, 2020).
52. Bateman, R.M., DiMichele, W.A. Escaping the voluntary constraints of “tyre-track” taxonomy. *Taxon* 70, 1062–1077 (2021).
53. Balme, B.A., Fossil in situ spores and pollen grains: an annotated catalogue. *Rev. Palaeobot. Palynol.* 87, 81–323 (1995).
54. Berdugo, M. et al. Global ecosystem thresholds driven by aridity. *Science* 367(6479), 787–790 (2020).
55. Müller, R.D., Cannon, J., Qin, X.D., Watson, R.J., Gurnis, M., Williams, S., Pfaffelmoser, T., Seton, M., Russell, S.H.J., Zahirovic, S. GPlates: building a virtual Earth through deep time. *Geochem. Geophys. Geosys.* 19, 2243–2261 (2018).

56. Blakey, R.C., Fielding, C.R. Gondwana paleogeography from assembly to breakup—A 500 my odyssey. *Geol. Soc. Am. Spec. Pap.* 441, 1–28 (2008).
57. Macdonald, F.A., Swanson-Hysell, N.L., Park, Y., Lisiecki, L., & Jagoutz, O. Arc-continent collisions in the tropics set Earth's climate state. *Science* 364, 181–184 (2019).
58. Hsieh, T.C., Ma, K.H., & Chao, A. iNEXT: an R package for rarefaction and extrapolation of species diversity (Hill numbers). *Meth. Ecol. Evol.* 7, 1451–1456 (2016).
59. Dunne, E.M. et al. Diversity change during the rise of tetrapods and the impact of the 'Carboniferous rainforest collapse'. *Proc. R. Soc. B.* 285, 20172730 (2018).
60. Alroy, J. Limits to species richness in terrestrial communities. *Ecol. Lett.* 21, 1781–1789 (2018).
61. Alroy, J. On four measures of taxonomic richness. *Paleobiology* 1–18 (2020).
62. Berner, R.A. A model for atmospheric CO<sub>2</sub> over phanerozoic time. *Am. J. Sci.* 291 (1991).
63. Berner, R.A. GEOCARB II: A revised model of atmospheric CO<sub>2</sub> over phanerozoic time. *Am. J. Sci.* 294 (1994).

## Declarations

### Acknowledgements

We thank those who have contributed to the plant and tetrapod data obtained from the Palaeobiology Database and the Global Biodiversity Information Facility. This research was supported by the NSFC Natural Science Foundation of China (grant 92055201). Zhen Xu is funded by the China Scholarship Council (202106410082) and the Natural Environment Research Council (UK) Biosphere Evolution, Transition and Resilience (BETR) program (grant NE/P0137224/1). BJWM and SWP are funded by the UK Natural Environment Research Council (NE/S009663/1). BJA is funded by an ETH+ grant (BECCY).

### Author Contributions

Z.X., J.X.Y., H.F.Y., and B.J.W.M. designed the study. Z.X. collected the plant dataset, and Z.X. and J.H. normalized and analyzed the plant dataset for the vegetation reconstruction. B.J.A. calculated the plant squared and interpolated diversity. A.S.M. produced the python code for the palaeogeographic reconstruction. B.J.W.M. and Z.X. modified and ran the SCION model. Y.G. and Y.D. provided FOAM climate model datasets and discussion of weathering processes. All authors contributed to the interpretations and conclusions, and Z.X. and B.J.W.M. wrote the paper with contributions from all co-authors.

## Competing interests

The authors declare no competing interests

## Figures

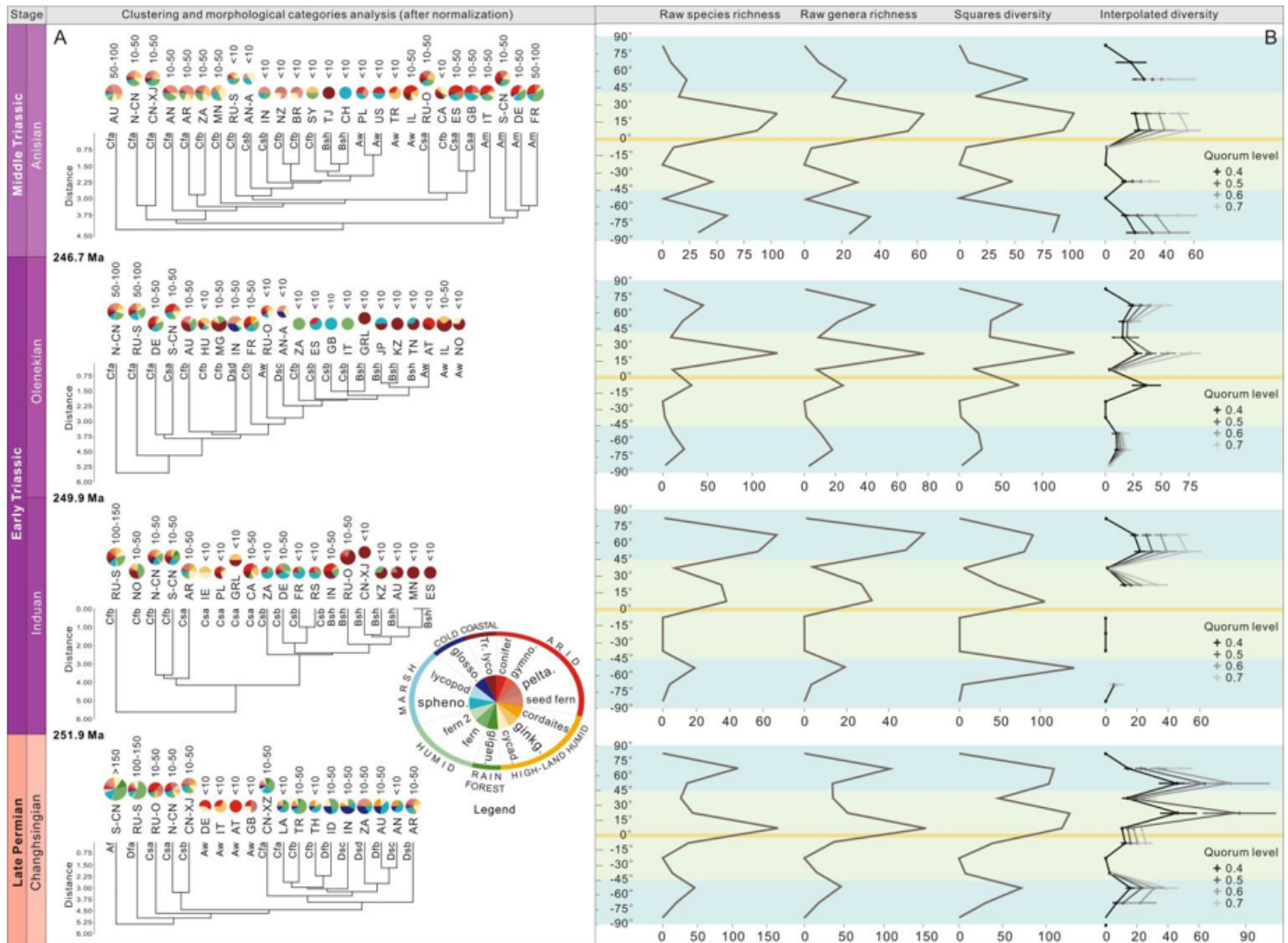


Figure 1

**Late Permian to Middle Triassic plant family level clustering, morphological categories and species richness by latitude (see original data in the Supplementary Information Tables S1, S4 and S5). All data used in this figure are normalized for fragmentation (see text). A.** Trees show clustering of flora in each area by plant family composition, with the corresponding climate zone abbreviation listed on the branches (e.g., Cfa, Cbf, etc. see Table S2 for all definitions). The pie chart above each branch shows the distribution of habitats within the morphological category, with the number of species shown above the

pie chart to indicate reliability of the result. Areas lacking macro plant fossil records do not have associated branches and are classified using palynology data. Area abbreviation: AN (Antarctica), AN-A (Aruba), AR (Argentina), AT (Austria), AU (Australia), BR (Brazil), CA (Canada), CH (Switzerland), CN-XJ (Xinjiang, China), CN-XZ (Xizang, China), N-CN (North China), S-CN (South China), DE (Germany), ES (Spain), FR (France), GB (United Kingdom), GRL (Greenland area), HU (Hungary), ID (Indonesia), IE (Ireland), IL (Israel), IN (India), IT (Italy), JP (Japan), KZ (Kazakhstan), LA (Laos), MG (Madagascar), MN (Mongolia), NO (Norway), NZ (New Zealand), PL (Poland), RS (Serbia), RU-S (Russia Siberia), RU-O (Russia excluding Siberia), SY (Syria), TH (Thailand), TJ (Tajikistan), TN (Tajikistan), TR (Turkey), US (United States of America), ZA (South Africa). Legend abbreviation: gymno. (gymnosperm), pelta. (peltasperm), ginkg. (ginkgophyte), cycad. (cycadophyte), gigan. (gigantopterid), spheno. (sphenophyte), glosso. (glossopterid), Tr. Lyco. (Triassic lycopod). **B.** All macro plant fossil species richness, genera richness, squares diversity and interpolated diversity (from left to right) are plotted in 15 degree latitude bins for each stage. Horizontal coordinates show taxa number and vertical coordinates show latitude. Blue and green areas show 'high latitudes' (-45°--90° and 45°-90°) and 'low-middle latitudes' (-45°-45°). Bins with less than three species have been plotted as '0', while missing points indicate an estimated diversity of more than three times the observed value. Error bars indicate 95% confidence intervals.

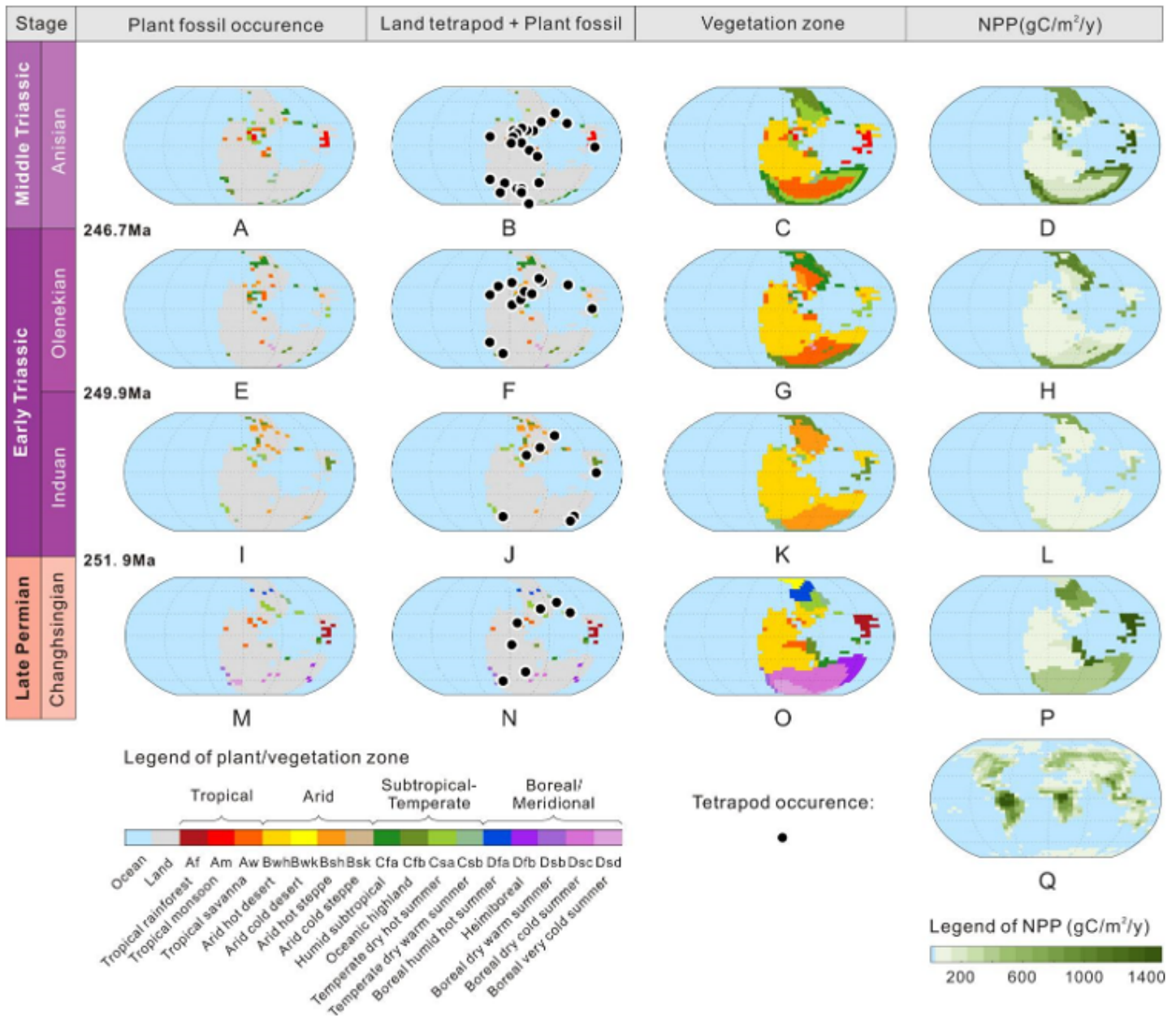
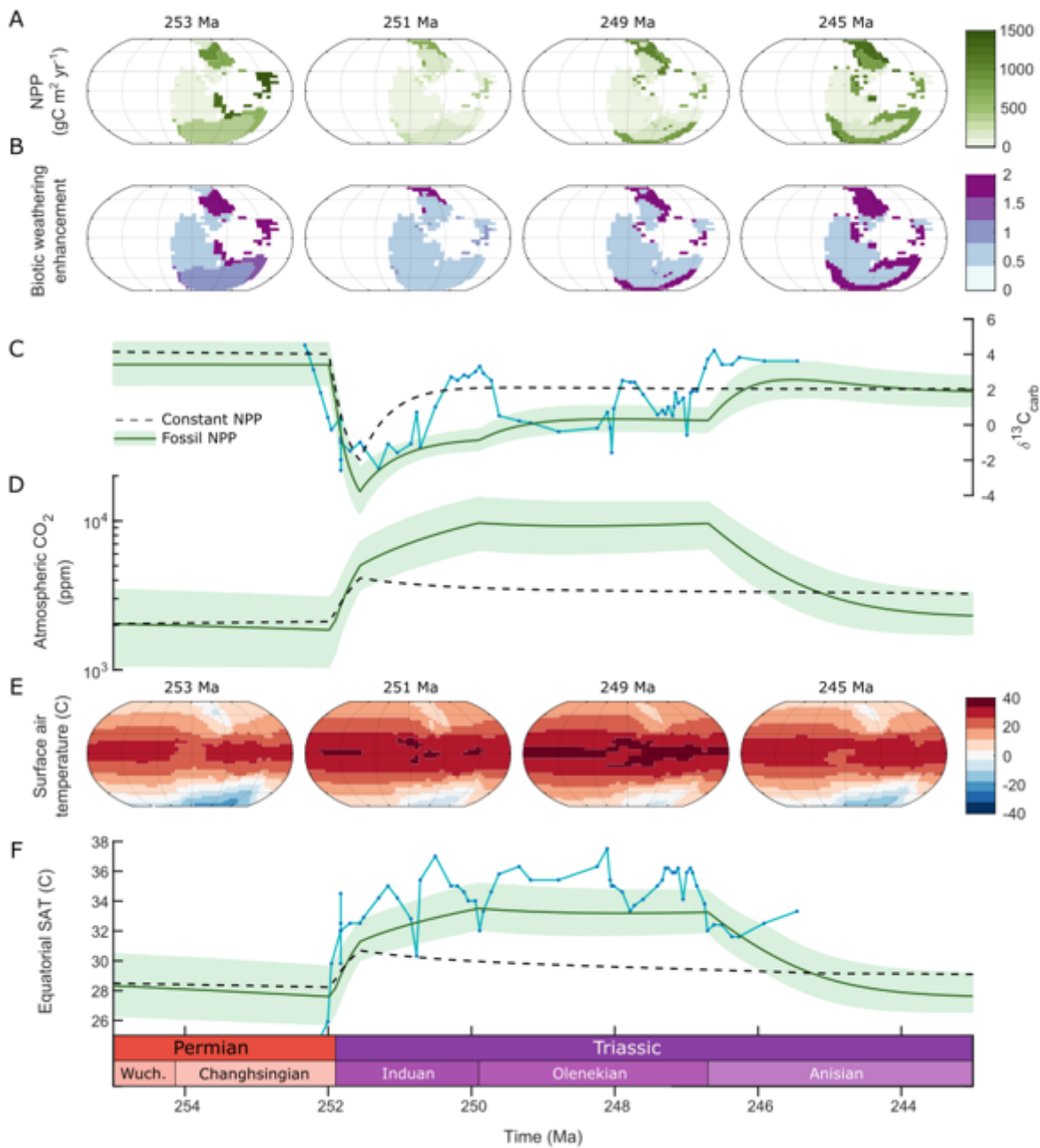


Figure 2

**Late Permian to Middle Triassic maps of plant and land tetrapod fossil records, vegetation reconstruction and Net Primary Productivity (NPP) distribution (see Supplementary Information for details).** 'Plant fossil occurrence' represents raw plant fossil data (Supplementary Information Tables S4 and S5), 'Land tetrapod+Plant fossil' represents terrestrial tetrapod occurrence data superimposed on land plant fossil data (Supplementary Information Table S6), 'Vegetation Zone' is the interpolation of that data using lithological indicators of climate zonation (Supplementary Information Table S2), and NPP is reconstructed based on the present day (Supplementary Information Table S3). End Permian Changhsingian: M, N, O, P; Early Triassic Induan: I, J, K, L; Early Triassic Olenekian: E, F, G, H; Middle Triassic Anisian: A, B, C, D; Modern world: Q. All maps are centered around 0,0.



**Figure 3**

**Climate-biogeochemical model driven by terrestrial NPP changes.** The vegetation NPP is prescribed onto the land surface in the SCION model (A), and affects the model calculations for organic carbon burial and the biotic enhancement of continental weathering (B). The model is run with (green solid line) and without (black dashed line) the fossil-prescribed NPP, where both models include the Siberian Traps degassing. C. Carbonate  $\delta^{13}\text{C}_{\text{carb}}$  compared to the dataset of ref Sun et al. (2012) (blue solid line with points). D. Atmospheric  $\text{CO}_2$ . E. Surface air temperature at chosen timepoints. F. Equatorial surface air temperature (SAT) compared to the equatorial SSTs of ref Sun et al (blue solid line with points).

## Supplementary Files

This is a list of supplementary files associated with this preprint. Click to download.

- [SupplementaryInformation.docx](#)